PCCP

Laser Ablation Syntheses of OThS and OCeS and their Characterization by Rotational Spectroscopy

Journal:	*Physical Chemistry Chemical Physics*
Manuscript ID	CP-ART-11-2024-004382.R1
Article Type:	Paper
Date Submitted by the Author:	17-Dec-2024
Complete List of Authors:	Isert, Joshua E.; Missouri University of Science and Technology, Department of Chemistry Davies, Alexander; Missouri University of Science and Technology, Department of Chemistry Grubbs II, Smitty ; Missouri University of Science and Technology, Chemistry Cooke, Stephen; Purchase College

ARTICLE

Laser Ablation Syntheses of OThS and OCeS and their Characterization by Rotational Spectroscopy

Received 00th January 20xx,
Accepted 00th January 20xx

DOI: 10.1039/x0xx00000x

Joshua E. Isert,[a] Alexander R. Davies, [a] G. S. Grubbs II[a] and S. A. Cooke [*b]

For the first time, rotational constants along with centrifugal distortion constants have been determined for OThS and OCeS. The rotational spectra of these molecules and, in each case, one other isotopologue ($OTh^{34}S$ and $O^{142}CeS$) were produced utilizing a laser ablation sourcing technique incorporated into a chirped-pulse Fourier transform microwave spectrometer operating in the 8 to 18 GHz region of the electromagnetic spectrum. The bent structures determined are in very good agreement with theoretical calculations. Comparisons between atomic coordinates, bond lengths and angles, as well as the inertial defect are discussed.

Keywords: OThS, OCeS, Thorium spectroscopy, Cerium spectroscopy, Rotational spectroscopy

Introduction

Matrix isolation infrared spectroscopy on the OThS and OCeS systems has been performed by Huang *et al*.[1] That study produced OThS and OCeS by reacting the laser ablated metal of interest in the presence of sulfur dioxide, SO_2. That work claims that the *f*-orbitals play a role in the bonding, leading to stronger metal-to-oxygen/sulfur triple bonds than found in other systems. In order to gain further insight into the chemistry of these systems, OThS and OCeS became the focal point of this rotational spectroscopic study.

Many actinide-containing polyatomic species have been previously studied spectroscopically using matrix isolation techniques, for examples see references 2, 3 and 4. To our knowledge, pure rotational spectroscopic studies of thorium- or cerium-containing polyatomic molecules do not exist and actinide-containing molecules, as a whole, are understudied. This work, then, begins with the study of OThS, the first gas phase study of an asymmetric thorium-centered polyatomic molecule. Furthermore, it is of interest to contrast the structures of thorium-containing compounds with those of cerium-containing compounds; cerium is one period above thorium on the periodic table. Cerium has a [Xe] $4f^1$ $5d^1$ $6s^2$ ground state electronic configuration compared to thorium, which is [Rn] $6d^2$ $7s^2$. This work, then, also reports the first pure rotational spectroscopy study of OCeS.

Experimental

Pure rotational spectra of OThS and OCeS were observed utilizing a laser ablation sourcing technique integrated into a CP-FTMW spectrometer operating at the Missouri University of Science and Technology (MS&T).[5,6] Samples of the spectra collected for these experiments are presented in Figures 1, 2, and 3. A gas mixture of approximately 0.1% carbonyl sulfide (OCS) in argon was pulsed at a 3 Hz rate through a Parker-Hannifin™ Series 9 solenoid valve to entrain the molecules in a collision free expansion into a vacuum chamber held at approximately 10^{-6} torr. Each gas pulse immediately interacts with a metal plasma produced by ablating a rotating and translating metal rod with the focused output of the 1064 nm fundamental wavelength of the Nd:YAG laser (Continuum™ Minilite II). The molecules produced then enter the vacuum chamber in a free-jet expansion between two horn antennae, with one broadcasting 4 μs linear sweeps of electromagnetic radiation spanning the 8 – 18 GHz region onto the molecules. These sweeps were originally power amplified to 10 W, and later to 40 W to gain signal on lower intensity transitions for the thorium spectrum. The cerium spectrum was obtained utilizing 10 W power amplification. Three free induction decays (FIDs) are collected per nozzle pulse and are averaged together for approximately 1 million acquisitions to minimize noise. Typical full width half maximum (FWHM) for these transitions were 80 kHz with a 10 kHz uncertainty attributed to the line centers as determined by previous experiments performed on this instrument.

[a] *Missouri University of Science and Technology, Department of Chemistry, 104 Schrenk Hall, 400 W. 11th St, Rolla, MO, 65409, U.S.A.*
[b] *Purchase College SUNY, School of Natural and Social Sciences, 735 Anderson Hill Rd, Purchase, NY, 10577, U.S.A.*

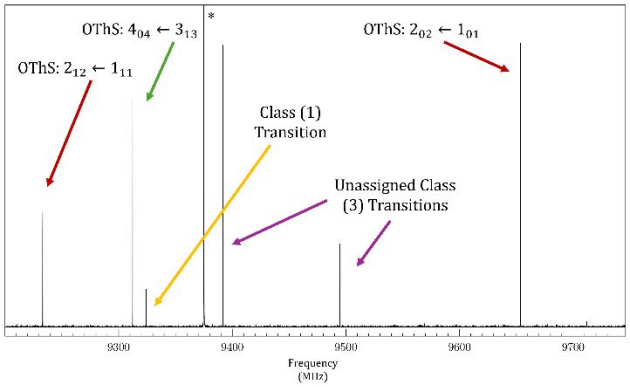

Figure 1: A sample of the collected spectrum with the laser ablated thorium rod in the presence of OCS. Red arrows represent the *a*-type transitions, the green arrow represents a *b*-type transition, the orange arrow represents a Class (1) transition, and the purple arrows represent Class (3) transitions that are yet to be assigned to a species. The signal marked with the asterisk located at 9375 MHz is an electronic artifact of the oscilloscope.

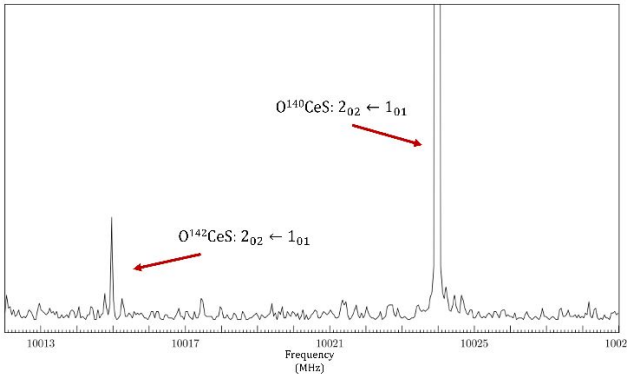

Figure 2: A portion of the spectrum for laser ablated cerium in the presence of OCS. The maximum intensity of the $O^{140}CeS$ transition has been cut off for easier visualization of the $O^{142}CeS$ transition.

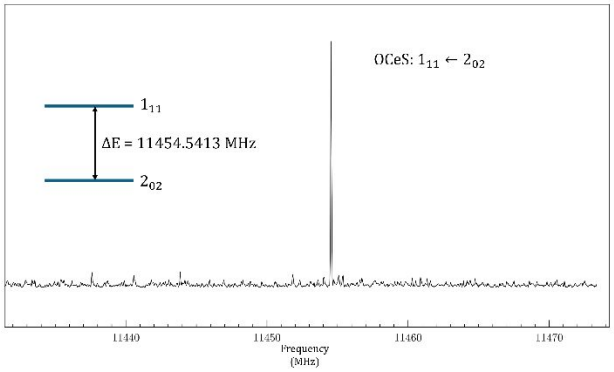

Figure 3: The *P*-branch, *b*-type transition assigned to the OCeS parent species. The 1_{11} level can be approximated as $\boldsymbol{A+B}$, while the 2_{02} level is approximately $\boldsymbol{2A+2B+2C-2[(B-C)^2+(A-C)(A-B)]^{1/2}}$.

Results and Analysis

The rotational transitions were recorded in the ground vibrational state of the ^{1}A' ground electronic state. When analyzing the rotational spectrum, one must be aware of the following being present in the scan: (1) transitions that do not require the laser ablation event, (2) transitions requiring the ablation event, but are independent of the metal being ablated, and (3) transitions requiring the laser ablation event and belong to the specific metal of interest. All three transition classes require the pulsing of the backing gas. Class (3) transitions will be those that are of experimental interest for these studies. Therefore, post processing involved elimination of classes (1) and (2) by overlaying the spectra collected under those conditions and only keeping lines of class (3) for further analysis. Class (3) transitions represent the only transition type utilized in this analysis. It is important to note that other lines of the class (3) variety are present in the spectra. Some of these transitions have been fit to other species,[7] but others remain unassigned to any molecular species at this time.

The OThS spectrum consisted of *a*-type and *b*-type transitions. A portion of the spectrum is displayed in Figure 1. When comparing the experimental rotational constants of $OTh^{32}S$ to the theoretical rotational constants[1], good agreement is observed, providing confidence in the reliability of the reported fits. In addition to this, rotational constants of the $OTh^{34}S$ species were also determined. The resultant spectroscopic constants for both isotopologues are presented in Table 1. In total, 25 rotational transitions were assigned in the 8 – 18 GHz region, with 18 transitions assigned to the parent species and 7 to the ^{34}S isotopologue.

The recorded laser ablated cerium spectra contained few class (3) transitions. One transition that became the focal point for the fitting of the $O^{140}CeS$ parent (^{140}Ce has a natural abundance of 88%) was the uncommonly observed *P*-branch, *b*-type transition $\mathbf{1_{11}\leftarrow 2_{02}}$ observed at 11454.5413 MHz. This transition is presented in Figure 3. Once included in the fit with

Table 1: Pure rotational spectroscopic parameters of $OTh^{32}S$ and $OTh^{34}S$.

	Theoretical[a] $OTh^{32}S$	$OTh^{32}S$	Theoretical[a] $OTh^{34}S$	$OTh^{34}S$
A (MHz)	13577.002	13555.4230(39)[b]	13390.687	13493.118(21)
B (MHz)	2598.230	2633.1716(15)	2494.761	2507.8775(79)
C (MHz)	2180.876	2200.0018(11)	2102.966	2110.5436(38)
D_J (kHz)	-	0.574(36)	-	0.62(16)
d_1 (kHz)	-	-0.205(12)	-	-0.275(37)
Transitions	-	18	-	7
RMS[c] (kHz)	-	7.0	-	11.3

a Derived from an equilibrium structure calculated at the B3LYP/6-311+G(3df) level with the SDD pseudopotential for Th reported in reference 1.

b Numbers in parentheses are one standard deviation in units of the last significant figure.

c Microwave RMS defined as $\sqrt{\sum[(obs-calc)^2]/\#\ of\ Transitions}$.

other tentative transition assignments, the working rotational constants became predictive and allowed other transitions to be assigned with ease. Once the fit of the parent species was completed, the O^{142}CeS species was also fit (^{142}Ce has a natural abundance of 11%). The spectroscopic constants for both isotopologues are presented in Table 2. In total, 19 rotational transitions were assigned in the 8 – 18 GHz region, with 11 transitions assigned to the parent species and 8 to the ^{142}Ce isotopologue.

An iterative least-squares fit of spectroscopic constants to the observed rotational transition frequencies was performed using Pickett's SPFIT/SPCAT suite of programs.[8] The transitions assigned to OThS and OCeS are listed in Tables 3 and 4, respectively. The fits required A_0, B_0, C_0, D_J, and d_1 in a Watson S reduced Hamiltonian[9] in the I^r representation for OThS, with the addition of D_{JK} for OCeS. When compared to the theoretical constants obtained through the works of reference 1, the experimental spectroscopic constant values for all species in this work are in very good agreement.

Discussion

The experimentally determined constant D_J has a higher uncertainty for the OTh^{34}S molecule than the other spectroscopic constants. However, when removed, the uncertainty of the other constants increased by an order of magnitude and the microwave RMS nearly doubled. Fixing the value to that of the OTh^{32}S parent species yielded an increased microwave RMS. Owing to the lack of success when attempting to change combinations of centrifugal distortion constants, it was determined that the somewhat large error was acceptable to produce a successful fit.

Table 2: Pure rotational spectroscopic parameters of O^{140}CeS and O^{142}CeS.

	Theoretical[a] O^{140}CeS	O^{140}CeS	Theoretical[a] O^{142}CeS	O^{142}CeS
A (MHz)	28065.6	24119.514(14)[b]	27985.8	24050.818(18)
B (MHz)	2569.4	2641.1538(30)	2567.5	2639.0381(36)
C (MHz)	2353.9	2372.1084(41)	2251.7	2369.7250(31)
D_J (kHz)	-	1.268(79)	-	1.289(76)
D_{JK} (kHz)		-77.27(45)		-76.7(18)
d_1 (kHz)	-	0.344(92)	-	[0.344][d]
Transitions	-	11	-	8
RMS[c] (kHz)	-	7.75	-	7.03

a Derived from an equilibrium structure calculated at the B3LYP/6-311+G(3df) level with the SDD pseudopotential for Th reported in reference 1.

b Numbers in parentheses are one standard deviation in units of the last significant figure.

c Microwave RMS defined as $\sqrt{\sum[(obs-calc)^2]/\#\ of\ Transitions}$.

d Number in square brackets is held to parent value.

Table 3: Observed and calculated transition frequencies of OTh^{32}S and OTh^{34}S.

$J'_{K-1\,K+1} \leftarrow J''_{K-1\,K+1}$	OTh^{32}S		OTh^{34}S	
	ν_{obs} (MHz)	$\Delta\nu$ (kHz)[a]	ν_{obs} (MHz)	$\Delta\nu$ (kHz)[a]
$2_{12} \leftarrow 1_{11}$	9233.1640	-1.1	8839.4895	-7.8
$4_{04} \leftarrow 3_{13}$	9312.2532	7.4	-	-
$2_{02} \leftarrow 1_{01}$	9653.7051	6.7	-	-
$2_{11} \leftarrow 1_{10}$	10099.4963	4.6	-	-
$1_{10} \leftarrow 1_{01}$	11355.4300	9.5	11382.5691	-4.0
$2_{11} \leftarrow 2_{02}$	11801.2185	4.7	-	-
$3_{12} \leftarrow 3_{03}$	12493.3838	2.0	-	-
$4_{13} \leftarrow 4_{04}$	13459.3486	-6.9	-	-
$3_{13} \leftarrow 2_{12}$	13841.9446	0.7	13252.7189	22.9
$3_{03} \leftarrow 2_{02}$	14449.0163	5.4	13812.8946	-16.1
$3_{22} \leftarrow 2_{21}$	14499.4479	-10.2	-	-
$3_{21} \leftarrow 2_{20}$	14549.8876	-17.9	-	-
$5_{14} \leftarrow 5_{05}$	14733.8439	-6.1	-	-
$5_{05} \leftarrow 4_{14}$	14786.7660	-0.3	13553.9593	-0.9
$3_{12} \leftarrow 2_{11}$	15141.1882	9.3	-	-
$1_{11} \leftarrow 0_{00}$	15755.4236	0.2	-	-
$6_{15} \leftarrow 6_{06}$	16356.1691	3.2	15919.1596	5.7
$4_{14} \leftarrow 3_{13}$	18441.6751	-2.7	-	-
$7_{16} \leftarrow 7_{07}$	-	-	17728.6116	-2.5

a $\Delta\nu = \nu_{obs} - \nu_{calc}$

Table 4: Observed and calculated transition frequencies of O^{140}CeS and O^{142}CeS.

$J'_{K-1\,K+1} \leftarrow J''_{K-1\,K+1}$	O^{140}CeS		O^{142}CeS	
	ν_{obs} (MHz)	$\Delta\nu$ (kHz)[a]	ν_{obs} (MHz)	$\Delta\nu$ (kHz)[a]
$2_{12} \leftarrow 1_{11}$	9757.7509	-7.7	9748.4801	-9.4
$2_{02} \leftarrow 1_{01}$	10023.9668	-5.5	10014.9547	-5.7
$2_{11} \leftarrow 1_{10}$	10295.8230	-4.3	10287.0837	-10.0
$6_{06} \leftarrow 5_{15}$	10322.7727	-3.6	-	-
$1_{11} \leftarrow 2_{02}$	11454.5413	-2.1	11396.9738	0.8
$3_{13} \leftarrow 2_{12}$	14635.0252	5.0	14621.1082	-0.8
$3_{03} \leftarrow 2_{02}$	15029.6085	2.6	15016.0660	11.0
$3_{22} \leftarrow 2_{21}$	15041.5167	12.5	-	-
$3_{21} \leftarrow 2_{20}$	15051.5323	-15.8	-	-
$3_{12} \leftarrow 2_{11}$	15442.0768	9.6	15428.9640	6.4
$7_{07} \leftarrow 6_{16}$	16021.1746	1.5	16057.5220	-0.8

a $\Delta\nu = \nu_{obs} - \nu_{calc}$

Likewise, the experimentally determined constant d_1 had a very high uncertainty for O^{142}CeS. Similarly, the removal of this constant resulted in a less than adequate fit. In this instance, the value of this constant was held to that of the parent molecule.

Due to the monoisotopic nature of thorium and low natural abundance of other isotopes, full substitution structures for both OThS and OCeS could not be obtained. However, because the parent and one minor isotopic species were successfully fit for each molecule, the coordinates of that particular atom can be determined using the Kraitchman equations[10] through the KRA program available on the PROSPE website.[11] In the case of OThS, the atomic coordinates of the sulfur atom are presented in Table 5. The same procedure was performed for the cerium atom in OCeS and the atomic coordinates are presented in Table 6. The substitution coordinates determined in this work agree well with the equilibrium coordinates derived from the theoretical structures.[1] The level of agreement gives confidence in the accuracy of the spectroscopic fits.

Effective structures have been calculated using the STRFIT[12] program and are presented in Tables 7 and 8. In order to generate the effective structure of OCeS, the cerium–oxygen bond was held constant to the computed structure found in reference 1. Typical covalent radii of single, double, and triple bonded molecules have been summarized.[13] Comparing these values to those of the effective structures allows for an estimation of the metal-chalcogen bond orders (see Table 7). In both cases, the metal–sulfur bond lengths found in this work appear closer to that of a double bond. Furthermore, the metal–oxygen bond length appears closer to a triple bond. This suggests that thorium and cerium can adopt a pentavalent nature. However, the computed structures[1] exhibited metal-to-oxygen/sulfur bond lengths that were both more consistent with triple bonds, showing the metals in a hexavalent bonding scheme. This represents the largest difference between the computed and experimental effective structures.

Table 5: Comparison of theoretical atomic position and Kraitchman[10] position of sulfur for OThS in the principal axis system.

	Theoretical (Å)[a]	This Work (Å)
a	2.20499	2.19843(69)[b]
b	0.31759	0.30373(494)

a Derived from an equilibrium structure calculated at the B3LYP/6-311+G(3df) level with the SDD pseudopotential for Th reported in reference 1.

b Numbers in parentheses are the Costain errors.[14]

Table 6: Comparison of theoretical atomic position and Kraitchman[10] position of cerium for OCeS in the principal axis system.

	Theoretical (Å)[a]	This Work (Å)
a	0.275446	0.2786(54)[b]
b	0.160983	0.1746(86)

a Derived from an equilibrium structure calculated at the B3LYP/6-311+G(3df) level with the SDD pseudopotential for Ce reported in reference 1.

b Numbers in parentheses are the Costain errors.[14]

Table 7: Double and triple covalent bond radii of M-O and M-S bonds

	This Work (Å)	Double Bond Radii (Å)[a]	Double Percent Error[b]	Triple Bond Radii (Å[a]	Triple Percent Error[b]
ThS	2.45	2.37	3.3%	2.31	5.7%
ThO	1.86	2.00	7.5%	1.89	1.6%
CeS	2.38	2.31	2.9%	2.26	5.0%
CeO	[1.78]	1.94	9.0%	1.84	3.4%

a Presented in reference 13.

b Percent error calculated as $|\boldsymbol{Pyykk\ddot{o}-This\ Work}|/\boldsymbol{This\ Work}*\mathbf{100}$.

c Bracketed values were held to that of the computed structure in reference 1.

Table 8 Comparison of theoretical and effective bond angles of OThS and OCeS.

	Theoretical[a]	This Work
OThS	116.3°	115.4(28)°[b]
OCeS	134.5°	130.1°(23)

a Derived from an equilibrium structure calculated at the B3LYP/6-311+G(3df) level with the SDD pseudopotential for Th and Ce reported in reference 1.

b Numbers in parentheses are one standard deviation in units of the last significant figure.

Additionally, the effective structures reveal bond angles of 115.4(28) degrees and 130.1(23) degrees for OThS and OCeS, respectively. The difference in angles is also reflected in the very different *A* rotational constants (see Figure 4 for a visualization and Tables 1 and 2 for the rotational constants, respectively). It has been shown previously that when in an A–B–A bonding scheme, the bond angle decreases as the polarizability of the central atom increases.[15,16] Cerium and thorium have polarizabilities of 205 a.u. and 217 a.u., respectively.[17] The slightly higher polarizability of thorium, then, suggests a smaller bond angle for OThS may be expected.

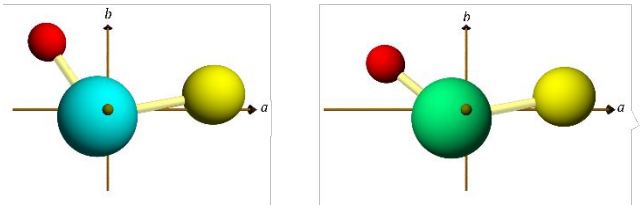

Figure 4: The OThS and OCeS molecules in the *ab*-principal axis plane. The O-Th-S angle is ~115 degrees whereas the O-Ce-S angle is ~130 degrees. The brown circle on the central metal atom represents both the location of the *c* axis and the center of mass.

The inertial defect, Δ, can also be used to gain structural insights for a molecular system. The inertial defect is given by $\boldsymbol{\Delta_0 = I_{cc}^0 - I_{aa}^0 - I_{bb}^0 = -2\sum_i m_i c_i^2}$, where $\boldsymbol{I_{aa}^0}$, $\boldsymbol{I_{bb}^0}$, and $\boldsymbol{I_{cc}^0}$ are vibrational moments of inertia about the *a*, *b*, and *c* axes in the ground vibrational state. Utilizing the PLANM program from the PROSPE[11] website, these inertial defects were calculated and have been presented in Table 9. For a rigid planar molecule, the value of Δ_0 will be zero. However, when leaving a rigid approximation, this value can be non-zero due to vibrational, centrifugal distortion, and electronic contributions. Vibrational contributions are typically the most significant. Herschbach and Laurie[18] have found that Δ_0 can be estimated for many different molecular systems. For a triatomic system, the inertial defect can be estimated by the equation $\boldsymbol{\Delta_0 = 4K/\omega}$, where $\boldsymbol{K = \frac{h}{8\pi^2} = 16.863}$ amu Å^2 cm^{-1} and ω is the wavenumber of the lowest energy vibrational mode. The lowest frequency vibration has been calculated in reference 1 for OThS to be the S-Th-O bend at approximately 146 cm^{-1}. The same has been done for OCeS, showing the S-Ce-O bend to be predicted at approximately 87 cm^{-1}. These values predicted from the inertial defects are presented in Table 9 and are compared with those calculated in reference 1, along with those found for SUO_2.[1]

Lastly, while the differences in structure have been outlined, this study is unable to verify the impact of the electronic structure of the central metal atom on these differences. It is noteworthy that the reactant gas used in this work was OCS, whereas in reference 1 the reactant gas was SO_2. It is likely that this speaks to the mechanism of the formation of the OThS and OCeS molecules. This finding is consistent with a mechanism in which the reactant gases are atomized during the laser ablation event. However, further studies would be required to verify this observation. Furthermore, it was observed that lowering the OCS concentration was necessary to bring about more intense class (3) transitions.

Conclusions

Pure rotational studies of the OThS and OCeS systems, along with a minor isotopologue for each, were successfully conducted. The spectroscopic constants determined through this work have a high level of certainty and very good agreement to theoretical strucures.[1] Furthermore, atomic coordinates of the substituted atom, an effective structure, and inertial defect values have been determined and compared. The class (3) transitions assigned in these experiments were few, and the investigation of those remaining is ongoing.

Table 9: Comparison of inertial defects and the lowest energy vibrational mode of the OThS and OCeS systems.

	Inertial Defect (amu Å^2)	Estimated ω (cm^{-1})	Literature ω (cm^{-1})
OThS	0.50725(16)	133	146[a]
OCeS	0.74962(43)	90	87[a]
SUO_2	0.410(3)[b]	165[b]	145[c]

a Derived from values found in reference 1.

b Derived from values found in reference 19.

c Derived from values found in reference 20.

Author contributions

Joshua E. Isert: Data Curation, Formal analysis, Investigation, Visualization, Writing – original draft, Writing – review & editing. **Alexander R. Davies:** Formal analysis, Supervision, Visualization, Writing – review & editing. **G. S. Grubbs II:** Conceptualization, Formal analysis, Funding acquisition, Investigation, Project administration, Resources, Supervision, Validation, Writing – review and editing. **S. A. Cooke:** Conceptualization, Formal analysis, Funding acquisition, Investigation, Software, Supervision, Validation, Visualization, Writing – review & editing.

Conflicts of interest

There are no conflicts to declare.

Data availability

The data supporting this article have been included as part of the manuscript.

Acknowledgements

This material is based upon work supported by the U.S. Department of Energy, Office of Science, Office of Basic Energy Sciences, Heavy Element Chemistry program under Award Number DE-SC0023242.

References

1 T. Huang, Q. Wang, W. Yu, X. Wang and L. Andrews, *Journal of Physical Chemistry A*, 2018, **122**, 5391-5400, DOI: 10.1021/acs.jpca.8b03731.
2 L. Andrews, Y. Gong, B. Liang, V. Jackson, R. Flamerich, S. Li and D. Dixion, *Journal of Physical Chemistry A*, 2011, **115**, 14407-14416, DOI: 10.1021/jp208926m.
3 P. Souter, G. Kushto, L. Andrews and M. Neurock, *Journal of Physical Chemistry A*, 1997, **101**, 1287-1291, DOI: 10.1021/jp962863d.
4 L. Andrews, H. G. Cho, K. Sahan Thanthiriwatte and D. Dixon, *Inorganic Chemistry*, 2017, **56**, 2949-2957, DOI: 10.1021/acs.inorgchem.6b03055
5 F. E. Marshall, R. Dorris, S. A. Peebles, R. A. Peebles, G. S. Grubbs II, *Journal of Physical Chemistry A*, 2018, **122,** 7385–7390, DOI: 10.1021/acs.jpca.8b05282
6 A. Duerden, F. E. Marshall, N. Moon, C. Swanson, K. M. Donnell and G. S. Grubbs II, *Journal of Molecular Spectroscopy*, 2021, **376**, DOI: 10.1016/j.jms.2020.111396.
7 J. Isert, J. Glenn, S. A. Cooke and G. S. Grubbs II, *Journal of Molecular Spectroscopy*, 2024, **406**, DOI: 10.1016/j.jms.2024.111952.
8 H. M. Pickett, *Journal of Molecular Spectroscopy*, 1991, **148**, 371-377, DOI: 10.1016/0022-2852(91)90393-O.
9 J. K. G. Watson, *Vibrational Spectra and Structure edited by J. R. Durig*, 1977, **6**, DOI: 10.1016/0022-2860(78)87040-9.

10 J. Kraitchman, *American Journal of Physics*, 1953, **21**, 17-24, DOI: 10.1119/1.1933338.
11 Z. Kisiel, *Spectroscopy From Space*, 2001, 91-106.
12 Z. Kisiel, *Journal of Molecular Spectroscopy*, 2004, **218**, 58-67, DOI: 0.1016/S0022-2852(02)00036-X.
13 P. Pyykkö, *Journal of Physical Chemistry A*, 2014, **119**, 2326-2337, DOI: 10.1021/jp5065819.
14 C. C. Costain, *Journal of Chemical Physics*, 1958, **29**, 864-874, DOI: 10.1063/1.1744602.
15 G. Linker, P. van Duijnen and R. Broer, *Journal of Physical Chemistry A*, 2020, ***124***, 1306-1311 DOI: 10.1021/acs.jpca.9b10248.
16 P. Debye, *Leipzig: Hirzel*, 1929.
17 P. Schwerdtfeger and J. K. Nagle, *Molecular Physics*, 2019, **117**, 1200-1225, DOI: 10.1080/00268976.2018.1535143.
18 D. R. Herschbach and V. W. Laurie, *Journal of Chemical Physics*, 1964, **40**, 3142-3153, DOI: doi.org/10.1063/1.1724977.
19 J. Isert, G. S. Grubbs II and S. A. Cooke, *Chemical Physics Letters*, 2024, DOI: 10.1016/j.cplett.2024.141726.
20 X. Wang, L. Andrews and C. J. Marsden, *Inorganic Chemistry*, 2009, **48**, 6888-6895, DOI: 10.1021/ic900869f.

Purchase College
STATE UNIVERSITY OF NEW YORK

Dr. Stephen A. Cooke
School of Natural and Social Sciences
Purchase College SUNY
November 17th, 2024

The data supporting this article, notably the measured spectroscopic transition frequencies, have been included as part of the manuscript.

Dr. Stephen A. Cooke: stephen.cooke@purchase.edu